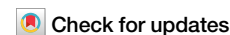


<https://doi.org/10.1038/s44304-026-00169-9>

Anthropogenic transition in flood regimes: insights from a millennium of the Yangtze River records

Yuanbo Liu^{1,2,3}✉, Ge Sun⁴, Jianguo Wu⁵✉, Yongwei Liu¹, Han Zhou⁶, Steven G. McNulty⁴ & Chenxi Liu⁷

Global floods are intensifying, yet climate change alone cannot resolve the persistent precipitation–flood paradox. Our millennial-scale analysis of the Yangtze River reveals that human activities, primarily deforestation and polder expansion, now outweigh climatic drivers in shaping flood regimes. This profound transition from natural to human-driven dominance necessitates a paradigm shift in risk prediction, prioritizing land-use dynamics to accurately capture extreme events that defy conventional hydrological expectations.

Flooding has impacted human society for millennia¹. Notable examples include the Judeo-Christian story of Noah's Flood² and the Chinese legend of Emperor Yu's Great Flood³, both of which underscore the profound societal impacts of such events. Floods still cause massive losses annually, e.g., the catastrophic 2022 Pakistan floods⁴, even though advancements in real-time satellite monitoring and hydrological models enable precise flood tracking, forecasting, and hindcasting^{5,6}. Many assessments suggest that floods will become more frequent and severe with global warming. However, empirical evidence to substantiate this conclusion remains surprisingly limited^{7,8}.

Floods are hydrological extreme events that often result from complex interactions between climate, hydrology, and human activities within a drainage basin⁹. Climate change has induced pronounced non-stationarity in hydro-climatic systems¹⁰, altering precipitation and runoff patterns globally, as evidenced by instrumental records spanning the past century^{8,11}. For instance, Europe experienced an unprecedented flood-rich period (1990–2016) that stands out even within a 500-year context¹². Paleo-flood reconstructions extending back two millennia further demonstrate that both flood-prone and quiescent periods have occurred across Europe and North America in either warmer or cooler climate intervals^{13–15}. Besides climate, human land use activities such as artificial channelization and land clearing were also qualitatively linked to increased flood frequency, e.g., in the Yangtze River since 1420 CE¹⁶. Land use change roughly accounted for 75% of the increased 100-year flood occurrences in the Mississippi River during the 20th century¹⁷. However, current studies lack a robust methodology to effectively disentangle the influences of anthropogenic and climate-driven factors on major floods, thereby sustaining ongoing scientific debates^{5,7}. For example, several studies suggest that deforestation and land

cover change primarily affect small to medium floods, while their influence diminishes for extreme events in large basins^{5,18–21}.

Furthermore, the precipitation–flood paradox—where observed and projected increases in precipitation extremes under climate change contrast with the mixed, and often non-increasing, trends in observed floods^{5,7,11}—highlights fundamental uncertainties in flood prediction arising from critical data and attribution gaps. Specifically, instrumental records (typically <100 years in most basins) are often too short to capture long-term flood variability, particularly for streamflow and precipitation extremes¹⁷. While historical documents could extend flood chronologies by millennia⁷, they remain underutilized due to concerns over data completeness, precision, and potential biases²². Similarly, paleo-flood reconstructions, though valuable, are inherently limited by the rarity of extreme events preserved in sedimentary archives, making it difficult to establish robust connections with climate proxies¹⁷. In flood attribution, historical records rarely document specific climate–flood linkages. Contemporary analyses of individual floods often focus on precipitation extremes but overlook the impacts of landscape change^{5,23}. Even when incorporated into numerical models, landscapes are typically parameterized empirically, with human activities treated as exogenous inputs, thereby obscuring their co-evolving nature and altering the catchment trajectory. Most critically, the pathways through which human activities modulate floods remain poorly understood and are rarely accounted for in flood risk projections. Particularly, land use changes may lead to potentially contradictory impacts on flood risk^{5,16,17,23}. Unfortunately, instrumental observations (<50 years) are often inadequate for evaluating and confirming hypothetical mechanisms behind infrequent events that occur over decades in slowly evolving landscapes^{19,21}. Collectively, these

¹Nanjing Institute of Geography and Limnology, Chinese Academy of Sciences, Nanjing, China. ²University of Chinese Academy of Sciences, Nanjing, Nanjing, China. ³University of Chinese Academy of Sciences, Beijing, Beijing, China. ⁴Eastern Forest Environmental Threat Assessment Center, USDA Forest Service, Durham, NC, USA. ⁵School of Life Sciences and School of Sustainability, Arizona State University, Tempe, AZ, USA. ⁶School of Resource and Environmental Engineering, Wuhan University of Technology, Wuhan, China. ⁷Institute for Design Innovation, Loughborough University London, London, UK.

✉e-mail: ybliu@niglas.ac.cn; Jingle.Wu@asu.edu

critical gaps significantly constrain our ability to reliably predict flood extremes, particularly for the most severe events.

To address these shortcomings, this study examined the Yangtze River Basin, where exceptional historical documentation provides flood history spanning over a millennium (950 CE to present) Box 1. This heavily populated basin represents both a historically flood-prone area with immense flood volumes²⁴ and a projected climate change hotspot for future flood risk⁵⁷. Moving beyond conventional event-centric analyses, we delineate emergent flood patterns through systematic integration of annually resolved historical records (950–2000 CE), encompassing flood chronologies, climatic variables (precipitation and temperature), and anthropogenic factors (population dynamics, forest cover changes, and

polder development) (see Methods). Our novel cascading attribution methodology advances flood causality analysis by decoupling dynamic and thermodynamic precipitation drivers, and then evaluates anthropogenic modifications to fundamental climate-flood relationships across this vast basin. These millennial-scale insights should deepen our understanding of flood variability and enhance our capacity for forecasting, mitigation, and integrated watershed management in a changing world.

Results

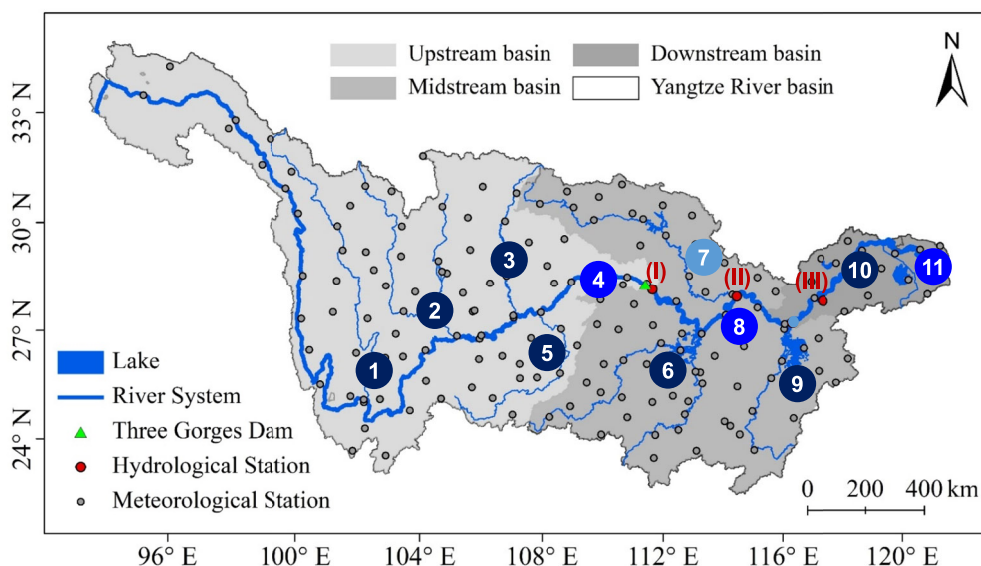
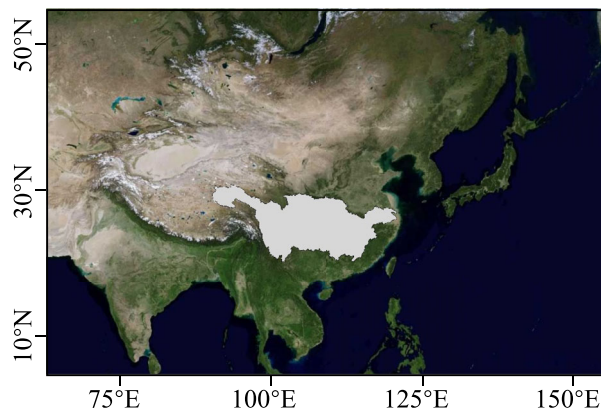
Millennial flood regimes in the Yangtze River Basin

The Yangtze River Basin, home to over 400 million people, has undergone distinct flood regime shifts during the past millennium. Our analysis of 1220

Box 1 | An overview of the Yangtze River Basin

The Yangtze River Basin covers an area of 1,800,000 km² (90°33'E–122°25'E, 24°30'N–35°45'N) (Box Fig. 1). The 6300-km long river flows from its source in the Tibetan Plateau in the west to its estuary in the East China Sea. The basin is characterized by a subtropical monsoon climate, with a multi-year average air temperature of 10.9°C and an annual precipitation of 1120 mm. The Yangtze River is classified as a temperate, humid-summer river, with a multi-year average annual

discharge of 900 km³ into the sea, accounting for 36% of China's water resources. Historically, flooding has been the most significant natural disaster in the region. The earliest quantitative record of flood-related human loss dates back to 185 BCE, as documented in The Book of Former Han. Hydro-climatological extremes have been consistently recorded in local chronicles, especially since the Sung Dynasty (960–1279 CE), by personnel authorized to document historical events.



- 1 Jinsha River
- 2 Mintuo River
- 3 Jialing River
- 4 Upper-mainstream
- 5 Wu River
- 6 Dongting Lake
- 7 Han River
- 8 Mid-mainstream
- 9 Poyang Lake
- 10 Down-mainstream
- 11 Yangtze Delta

Box Fig. 1 Geophysical location of the Yangtze River basin. Three key representative locations are shown: Yichang (I), Hankou (II), and Datong (III), progressing from the upper to the downstream regions. The Three Gorges Dam is positioned 40 km upstream of Yichang. The basin currently has 179 national meteorological stations distributed across 11 sub-basins.

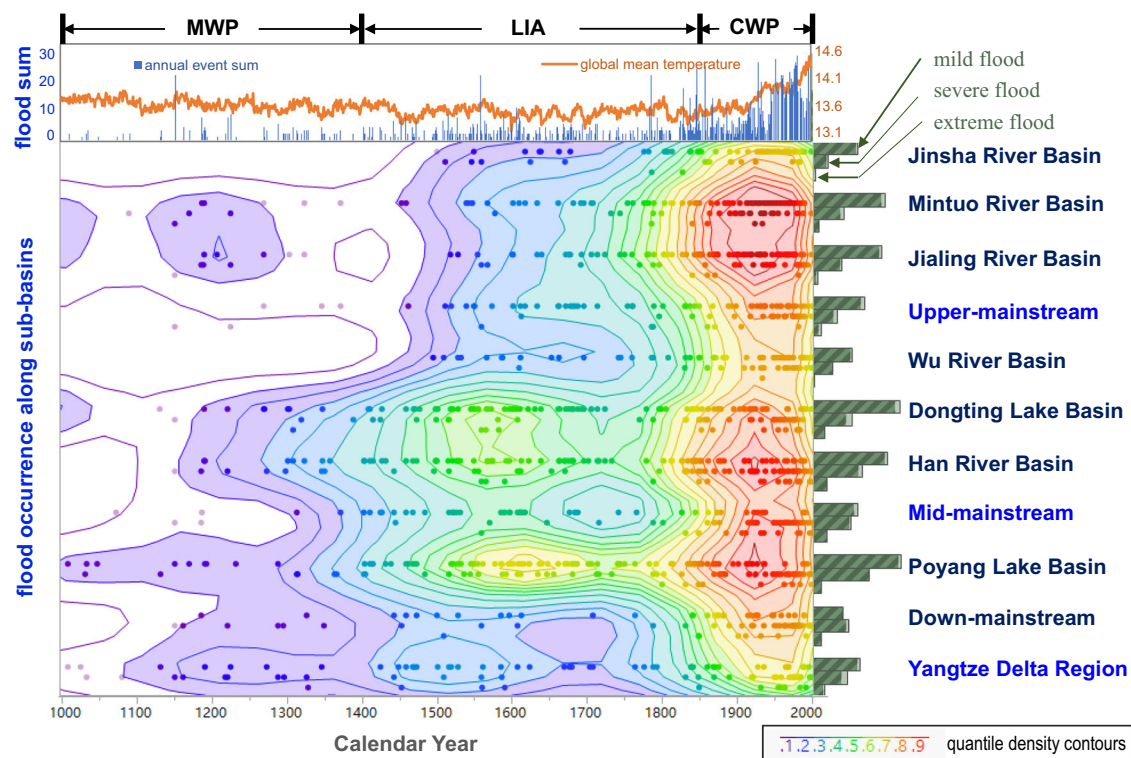


Fig. 1 | Flood occurrences across the 11 sub-basins of the Yangtze River Basin, from the upper to the lower reaches, span the Medieval Warm Period (MWP), the Little Ice Age (LIA), and the Current Warm Period (CWP) from 1000 to 2000 CE. The upper plot illustrates the variation in annual global temperature alongside the total annual flood occurrences. The lower panel presents flood regimes, with each

point representing a flood event. Quantile density contours at 5% intervals are shaded from pink (5%) to red (95%), illustrating the gradient from poor to rich regimes. The right plot displays a histogram categorizing floods into mild, severe, and extreme for each sub-basin over the entire period.

historically documented flood events across 11 sub-basins is classified into three severity categories: mild (Group 1), severe (Group 2), and extreme (Group 3) floods. These events delineate three flood regimes corresponding to major climatic epochs: the Medieval Warm Period (MWP; 950–1400 CE), the Little Ice Age (LIA; 1400–1850 CE), and the Current Warm Period (CWP; 1850 CE–present), yet the transitions between flood-poor and flood-rich periods are less pronounced (Fig. 1) than the nine regularly recurring flood-rich periods identified in European records¹². The basin shows clear nonstationary behavior in flood regime (Table 1), with an exponential increase in both annual flood frequency and number of affected sub-basins (~3.5% annual growth rate), alongside a 56% intensification in mean flood magnitude during the past two centuries, despite potential underreporting of early mild and severe events (Fig. S1). Spatially, the affected sub-basins were initially confined to downstream areas, but over time, the impacts expanded to upstream sub-basins as well, with two distinct flood hotspots emerging in terms of flood density (events per region per period) (Fig. 1). One is the persistently active middle reaches (Han River and Poyang Lake basins). Another is the upper reaches (Mintuo River and Jialing River basins), where floods intensified in both warm climatic periods. These patterns indicate a general trend toward more frequent and severe floods, underscoring the inadequacy of assuming flood stationarity for engineering design and watershed management planning. The observed intensification warrants a comprehensive investigation of its climatic and anthropogenic origins in this river system, which is globally significant due to its large size, high population dependence, and socio-economic importance.

Climatic origin of flood regimes

Floods originate primarily from basin precipitation. In the Yangtze River Basin, located within the Asian monsoon-dominated region, most floods occur during the summer rainy season²⁵. The river basin experiences dry or wet climatic conditions, classified into six distinct precipitation modes for May

through August, based on comprehensive documentation and climate data in China spanning from 950 to 2000 CE^{26–28} (Fig. S2). Climate change can impact regional precipitation, and thus floods, through both thermodynamic (primarily through temperature-driven increases in moisture capacity) and dynamic mechanisms (via alterations in atmospheric circulation patterns)^{29–31}.

As a result of dynamic shifts in large-scale atmospheric circulation³², particularly changes in the East Asian monsoon and mid-latitude westerlies, wet precipitation regimes became most common during the LIA (Fig. 2a). Under colder global conditions, the subtropical westerly jet stream weakened and shifted equatorward, enhancing meridional flow and moisture transport into East Asia^{32,33}. This southward displacement fostered persistent rain belts and increased flood frequency through a “flood-rich” mechanism, as blocking patterns slowed the progression of weather systems. Additionally, the western North Pacific subtropical high may have intensified and extended westward, further reinforcing monsoonal moisture convergence over the region³⁴. Comparable mechanisms have been associated with contemporaneous flood-rich periods in Europe, where polar jet stream shifts and amplified meridional flow sustained quasi-stationary weather systems and extreme precipitation^{12,35}. Despite some hemispheric coherence, these interactions underscore strong regional controls on precipitation regimes, which vary substantially across climate zones and limit global uniformity of flood signals. Notably, LIA precipitation exhibited a reduced frequency of multi-decadal oscillations (Fig. 3a), indicating suppressed atmospheric variability under colder climates³⁶. Such suppression diminishes the intensity and frequency of oscillatory phenomena, such as monsoon fluctuations and ENSO-related anomalies, thereby promoting more persistent and stable atmospheric states^{37,38}. These stabilized conditions likely contributed to more uniform precipitation regimes, shaping the observed multi-decadal flood variability and leading to a higher frequency of mild floods relative to severe events during this period (Fig. 2b).

Unlike dynamic circulation shifts, thermodynamic changes in precipitation exert distinct influences on flood regimes through temperature-

Table 1 | Stationarity test of time series (x_t) using the Augmented Dickey-Fuller (ADF) test, including decomposed approximate coefficients for four flood indices, global mean temperature, China's precipitation regime, and polder area in the Yangtze River Basin from 950 to 2000 CE

ADF t-statistic	Constant, Linear trend			Constant			None			Order of integration
	x_t	Δx_t	$\Delta^2 x_t$	x_t	Δx_t	$\Delta^2 x_t$	x_t	Δx_t	$\Delta^2 x_t$	
Annual flood sum	-0.2850	-9.6753 (***)		1.7991	-9.0177 (***)		2.4303	-8.6825 (***)		(1)
Annual flooded basin	0.9908	-9.1460 (***)		2.4348	-8.3322 (***)		2.9789	-7.9742 (***)		(1)
Overall flood intensity	-3.1266	-9.1092 (***)		-0.7714	-8.9627 (***)		0.1713	-8.8672 (***)		(1)
100-year flood density	-1.8412	-28.0179 (***)		1.1138	-27.8932 (***)		2.8500	-27.6763 (***)		(1)
Global mean temperature (T)	-2.3068	-21.4404 (***)		-2.4386	-21.3905 (***)		0.4737	-21.3904 (***)		(1)
Precipitation regime (P)	-27.4758 (***)	-21.0486 (***)		-27.4608 (***)	-21.0589 (***)		-1.5759	-21.0689 (***)		(1)
Population (Po)	0.2468	-1.9118	-32.3913 (***)	1.8517	-0.9615	-32.3657 (***)	2.1770	-0.3983	-32.3570 (***)	(2)
Forest cover (Fc)	0.2287	0.5898	-34.8369 (***)	-1.7736	0.9403	-34.7077 (***)	0.5492	0.6289	-34.6776 (***)	(2)
Polder area (Pa)	-2.6983	-3.8077 (*)		-1.3877	-3.7119 (**)		1.3171	-2.9702 (**)		(1)

The null hypothesis assumes that x_t has a unit root, with the regression method being ordinary least squares (OLS) and three options for an exogenous regressor: (1) constant and linear trend, (2) constant, and (3) none. The ADF test is applied to x_t and its higher-order differences until the t-statistic becomes significant, which determines the order of integration for the series. The results indicate that all series are nonstationary (1) processes, except for population and forest cover, which are (2) processes. (***) (**), and (*) denote the test significance at the level of $p < 0.001$, < 0.01 , and < 0.05 , respectively.

mediated moisture availability. While cold climates favor wet precipitation regimes in the region, warming tends to increase precipitation, as predicted by Clausius-Clapeyron scaling^{39,40}. Historical records (1470–2000 CE) support this thermodynamic effect through differential trends: wet regimes exhibit stronger precipitation increases (7.6% per century for regime V) than dry regimes (3.4% for regime I) (Fig. 3b), comparable to reported precipitation–temperature scaling rates of approximately 7% per degree⁴¹. We refer to this warming-driven enhancement as a ‘flood-strong’ mechanism, meaning that rising temperatures amplify precipitation within existing regimes, thereby increasing flood severity without altering the underlying circulation state (Fig. 3c). In reality, dynamic and thermodynamic processes often interact, jointly shaping flood risk through both regime shifts and intensity amplification. Consequently, warming has reduced the frequency of mild floods while increasing severe and extreme events, suggesting a shift towards fewer mild but more intense floods. A similar thermodynamic amplification may also explain the recent surge in large floods across Europe¹². These consistent hemispheric patterns underscore thermodynamic scaling as a key contributor to contemporary flood intensification.

Overall, the dynamic and thermodynamic mechanisms of precipitation exert different impacts on flood frequency and magnitude. Together, they explain the known inconsistency between cold/warm climates and flood-rich/-poor periods¹², which can help better predict flood regimes in the context of climate change. However, these statistically stationary precipitation regimes account for <20% of observed millennial flood variability and fail to explain the pronounced exponential uptrends. Most strikingly, precipitation-normalized flood intensity increased by 23.5% during the Current Warm Period, significantly exceeding the levels of the Little Ice Age (Fig. 4), suggesting that factors beyond climate change have influenced floods in the region.

Increasing dominance of anthropogenic influences on flood regimes

Land use changes alter the natural hydrological properties of catchments, but their long-term impacts on floods are often speculative and not explicitly considered in current flood predictions^{7,8,42}. Our millennial-scale analysis, combining signal processing and cointegration regression, shows that human land use activities have surpassed climatic influences in exacerbating floods (Table 2, Figs. S3 and S4). Specifically, dynamically and thermodynamically driven precipitation variations contributed mainly to flood fluctuations. In contrast, growing anthropogenic influences were responsible for the observed uptrend in both flood frequency and intensity over the past 1000 years.

Traditional unit hydrograph theory assumes flood intensity scales proportionally with precipitation in a basin^{43,44}. However, our analysis of independent precipitation and flood datasets (1470–2000 CE) reveals that this fundamental assumption fails to hold ($R^2 = 0.03$) (Fig. 5a). By incorporating anthropogenic indicators (population density, forest cover, polder area) into the precipitation–flood relationship, we demonstrate that human activities fundamentally reconfigure flood generation mechanisms. Notably, normalization by these indicators restores statistical significance, with combined anthropogenic adjustments yielding an R^2 of 0.82 ($p < 0.0001$) (Fig. 5e). Forest cover emerges as the dominant mediator, accounting for 71% of variability when considered independently. The basin’s dramatic deforestation from 60% to 10% coverage over the millennium provides an exceptional trajectory to track these effects. Obviously, forests consistently reduce both flood frequency and intensity under equivalent precipitation - particularly for heavy floods (i.e., intensity ≥ 2) (Fig. 5f). The clear inverse relationship between forest cover and flood severity proves forests buffer floods across all event magnitudes even during extreme rainfall, thereby resolving the long-standing ‘forest-flood debate’ through irrefutable, observation-based evidence^{19,21}. Beyond this theoretical resolution, the restored precipitation–flood relationship under anthropogenic normalization ($R^2 = 0.82$) demands the urgent incorporation of land-use legacies into global flood risk assessments, particularly for those nations where deforestation continues unabated and parallels the Yangtze’s historical trajectory.

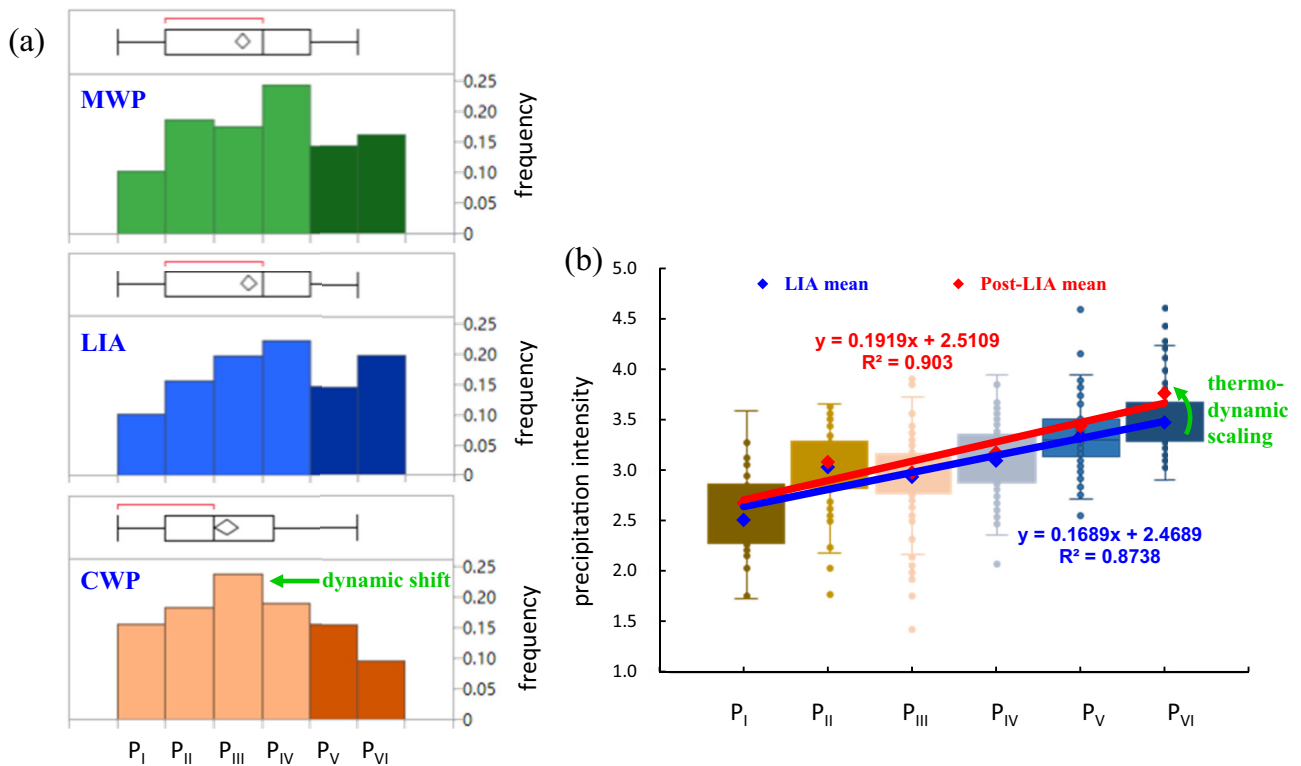


Fig. 2 | Climatic impacts on regional precipitation regimes through dynamic shifts and thermodynamic scaling. **a** Histogram of precipitation regimes in China, ranging from extreme dry (P_I) to extreme wet (P_{VI}), during the Medieval Warm Period (MWP), the Little Ice Age (LIA), and the Current Warm Period (CWP). Wet regimes were more prevalent during the LIA, while dry regimes dominated in the CWP, indicating a dynamic shift in precipitation patterns. **b** Box-whisker plots of

precipitation intensity across individual regimes in the Yangtze River Basin. Boxes represent the interquartile range, diamond markers indicate means, whiskers show variability, and individual data points are plotted. The MWP is excluded due to missing data prior to 1470. The difference between the regression lines for the LIA (blue) and the Post-LIA/CWP (red) indicates a thermodynamically driven increase in precipitation intensity, as confirmed by a two-tailed *T* test ($p = 0.0236$).

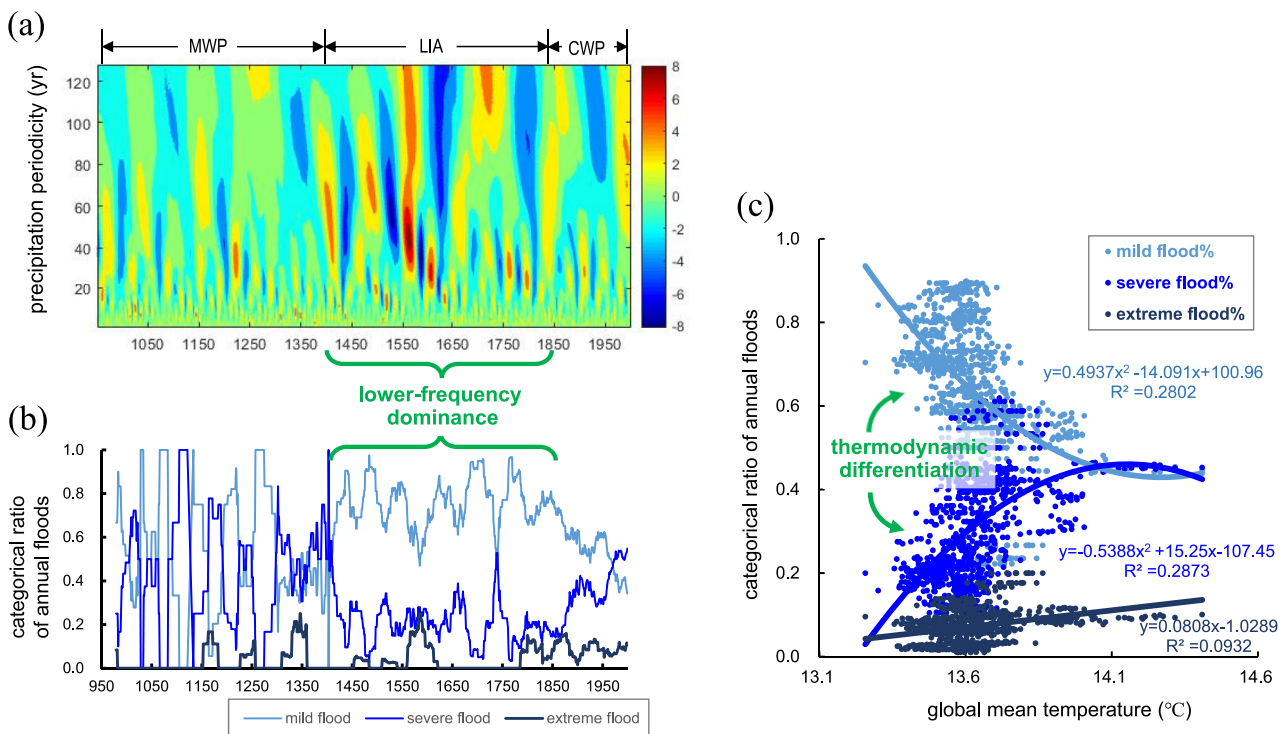
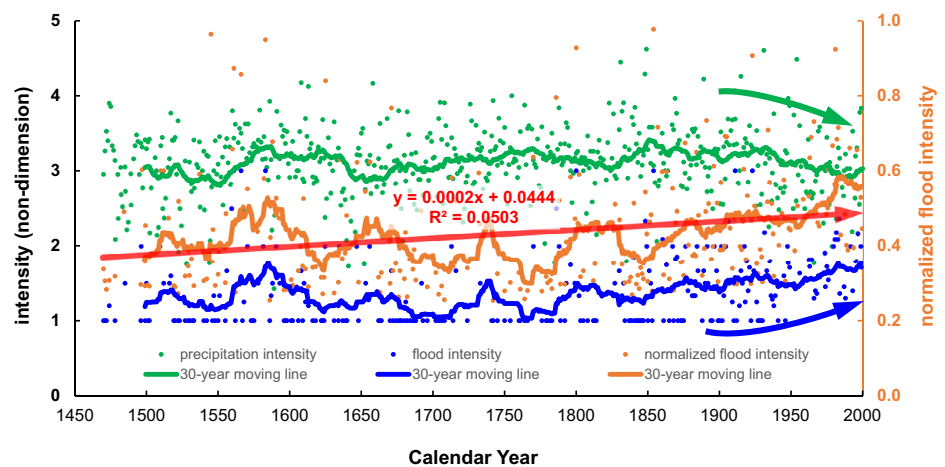


Fig. 3 | Climate impacts on Yangtze floods via dynamic and thermodynamic mechanisms in 950-2000 CE. **a** The continuous wavelet power spectrum of precipitation shows lower frequency precipitation patterns dominating during the Little Ice Age (LIA). **b** The categorical ratio of annual floods, smoothed with a 30-year moving

window, reflects flood frequency patterns similar to precipitation during the LIA. **c** The categorical ratio of annual floods correlates with rising global mean temperatures, showing a significant decrease in mild floods but an increase in severe and extreme floods, highlighting the thermodynamic differentiation in flood magnitude.

Fig. 4 | Fluctuations in precipitation intensity (green) and flood intensity (blue) in the Yangtze River Basin from 1470 to 2000 CE. The normalized flood intensity (orange), adjusted for precipitation, shows a pronounced upward trend (a 23.5% increase during the CWP compared to the LIA), suggesting that factors beyond precipitation change have significantly contributed to flood generation.



Apart from the deforestation trajectory, humans have a long history of cultivating agricultural fields, developing urban areas, and building hydraulic infrastructure to improve living conditions in flood-prone and low-lying areas⁴⁵. Major hydraulic solutions implemented in the Yangtze River Basin include polder systems, which entail constructing levees and drainage systems to prevent flooding within the area, as well as building banks and dams to regulate floodways. However, these hydraulic engineering measures may yield unintended consequences, such as raising riverbed levels, a phenomenon known as the levee paradox¹⁷. Our cointegration regression analysis demonstrates that afforestation tends to reduce overall floods, while population growth and polder expansion tend to increase floods (Figs. 6b, 7d). The impact of population growth is largely associated with urbanization, which increases built-up and paved areas, reducing soil infiltration capacity, increasing rapid runoff, and thereby elevating flood risk. Over the past millennium, the basin's population has increased tenfold, the polder area has expanded fivefold, and formerly separate polders have coalesced into large, interconnected hydraulic communities in an evolving way⁴⁶ (Fig. S3a). The drainage outflows from these systems elevate downstream water levels, pushing flood impacts further downstream¹⁹. This phenomenon became particularly evident during the early 1600s, when the peak of polder construction coincided with an increase in flood occurrences—occurring more often than expected in 9 out of 10 years⁴⁷. The problem has worsened with the shift from traditional human-powered water-wheels to modern high-capacity electric pumping systems, particularly in recent decades⁴⁸ (Fig. S3b). The current network of 2629 stations, with a combined drainage capacity of 19,400 m³/s (~25% of peak flood flows)⁴⁹, has substantially increased flood vulnerabilities in downstream regions containing major urban agglomerations such as Nanjing and Shanghai. This technological shift explains the disproportionate severity of recent catastrophic floods (1954, 1998, 2020) relative to their precipitation inputs (Fig. 6). Most strikingly, while the 1954 and 1998 floods occurred under comparable rainfall conditions, the 2020 event achieved record flood peaks with significantly less precipitation—clear evidence that artificial drainage systems have become the dominant flood driver in the contemporary period.

In summary, human activities have inadvertently but progressively altered landscapes while deliberately developing water infrastructure, jointly producing emergent flood dynamics (Fig. 7). This anthropogenic emergence requires a conceptual shift from natural to human-dominated flood risk prediction. Given the feedback nature between human interventions and flood systems, exemplified by the forest-flood debate, polder effects, and levee paradox, anthropogenic factors must be incorporated as endogenous variables rather than external drivers. The conceptual shift should foster the development of structurally novel models that enhance flood predictability. This is especially the case for “dragon-king” occurrences, which represent extreme outliers arising from distinct generating processes rather than

ordinary hydro-climatological variability and therefore deviate from standard hydrological expectations⁵⁰.

Future floods in the anthropocene

Climate projections from the IPCC AR6 indicate that global near-surface and air temperatures will continue to rise until at least mid-century, relative to 1850–1900 levels^{8,51}. According to projections from the Coupled Model Intercomparison Project Phase 6 (CMIP6), precipitation in the Yangtze River Basin is expected to increase in both annual totals and daily maximums under all emissions scenarios throughout this century⁵¹. The basin is expected to enter a wetter phase of its dominant precipitation cycle within the next 30–40 years. Coupled with thermodynamic intensification of precipitation, Yangtze floods are very likely to become more frequent and intense in the coming years. Superimposed on existing anthropogenic flood amplifiers, these hydrological changes pose substantial risks to this economically critical region, which sustains one-third of China's population and generates over 40% of the national GDP.

Discussion

Human-caused landscape changes, as well as climate change, must be explicitly considered in any effective flood-risk mitigation and resilience building. Reliable flood predictions depend on accurate attribution of dynamic (atmospheric circulation) and thermodynamic (temperature-mediated) precipitation changes that are currently lacking in structuring flood attribution. Equally critical is quantifying anthropogenic influences as endogenous variables in midterm flood risk prediction, which are currently treated as static in most models, despite their significant role in shaping flood regimes. Historical land-use baselines (e.g., the Yangtze's decline from 60% to 10% forest cover) can inform nature-based solutions, such as reforestation, while modern engineering impacts (e.g., a 19,400 m³/s pumping capacity) necessitate whole-basin management frameworks. Such frameworks should conceptualize the Yangtze as a coupled human-water system, where upstream interventions, such as deforestation, and downstream infrastructure, like polders, interact across scales. These findings can help improve flood prediction models by incorporating land-use legacies, develop next-generation early-warning systems that consider both climate and human factors, and implement adaptive policies that recognize the basin's evolving flood vulnerability. The findings of our study should have implications for global flood-prone regions under similar climates to the Yangtze.

Methods

Methodology

Unlike instrumental observations, historical records of heavy precipitation and flood events are often qualitative, with more quantitative descriptions appearing in later periods. Since the 1980s, historical events have been

Table 2 | Cointegration relationships between the time series of decomposed approximate coefficients for four flood indices and five forcing variables from 950 to 2000 CE

Time series (Y)	Cointegration relations with forcing variables (regression function)	R ²	Standardized coefficients for variables in regression				
			Global mean temperature (T)	Precipitation regime (P)	Population (Po)	Forest cover (Fc)	Folder area (Pa)
Annual flood sum	$Y = 2.834T - 0.025P + 1.273 \times 10^{-6}Po + 0.009Fc + 9.247 \times 10^{-6}Pa - 39.554$	0.771 (***)	0.273 (***)	-0.026	0.771 (***)	0.089	0.109 (*)
Annual flooded basin	$Y = 5.142T - 0.040P + 2.450 \times 10^{-6}Po + 0.046Fc + 2.250 \times 10^{-6}Pa - 73.723$	0.778 (***)	0.296 (***)	-0.026	0.886 (***)	0.288 (***)	0.158 (***)
Overall flood intensity	$Y = 0.503T + 0.003P + 2.339 \times 10^{-10}Po - 0.020Fc - 2.256 \times 10^{-6}Pa - 5.573$	0.719 (***)	0.208 (***)	0.012	0.061	-0.891 (***)	-0.114 (*)
100-year flood density	$Y = 35.370T - 0.224P - 1.739 \times 10^{-9}Po - 1.391Fc - 391.352$	0.839 (***)	0.246 (***)	-0.017	-0.008	-1.009 (***)	-0.123 (***)

The Johansen cointegration test confirmed the presence of multicointegration at $p = 0.05$ level, yielding relationships with high correlation coefficients ($R^2 > 0.71$). The standardized coefficients in the regression indicate the contributions of the forcing variables to the flood series, with higher absolute values representing greater contributions. The results demonstrate that anthropogenic factors (population growth, changes in forest cover, and folder expansion) have had a more significant impact on flood trends than climatic factors (temperature and precipitation).

(***), (**), and (*) denote the test significance at the level of $p < 0.001$, < 0.01 , and < 0.05 , respectively.

extensively compiled by Chinese national institutions using common criteria to classify events by magnitude^{26,52}. We accordingly assigned numerical values to the classes, ranging from 1 to 3 for documented flood magnitude (mild, severe, and extreme) and 1–5 for station-based summer precipitation (dry to wet). We also categorized precipitation into six regimes (I–VI) from dry to wet for the millennium in China. For floods, we calculated the number of annual events, the number of flooded sub-basins, and the flood frequency for the entire Yangtze River Basin. We used an exponential fit to the annual flood frequency and affected sub-basin trends to estimate their annual growth rates. In the absence of instrumental data for mainstream discharge and water levels, we defined the overall flood intensity of the entire basin as the mean magnitude of annual events. Relative to the previous eight centuries, flood intensification over the past two centuries was quantified using the mean flood magnitude. We also defined flood density as the total number of occurrences in a region during a specific time period to portray the spatiotemporal regime. To categorize flood severity, we calculated the ratio of annual floods within each severity class (mild, severe, and extreme floods) to the total number of floods for that year in the basin. Despite the well-established local chronicles system for event documentation dating back to the Sung Dynasty (960–1279 CE)^{52,53}, we scrutinized historical floods using an information-entropy-based test to ensure data robustness for statistical analysis (see Fig. S1 for details). This test evaluates the randomness and informational completeness of the event sequence by calculating entropy across time segments. Low entropy values suggest potential data gaps or reporting biases, whereas higher entropy indicates a more uniform and diverse distribution of events, reflecting greater completeness and reliability. For precipitation, we defined the overall precipitation intensity of the entire basin as the annual mean of the numerated summer precipitation for 32 stations available within the basin for 1470–2000 CE (Fig. S5). The overall intensity also serves as a basis for assessing the agreement between basin precipitation and continental dry-wet regimes (Fig. 2b).

To disentangle the impacts of climate change on floods using documented data, we decomposed the complex cascade from temperature to precipitation, to specific landscapes, and to individual flood events in three dimensions (cascading attribution). First, we analyzed precipitation variability from both dynamic and thermodynamic perspectives. Dynamically, we used the national annual dryness/wetness time series (950–2000 CE) to characterize regional precipitation regimes shaped by the Asian Monsoon and other large-scale atmospheric circulation systems (Fig. S2^{26–28}). Thermodynamically, we divided the dryness/wetness series into the Medieval Warm Period (950–1400 CE), the Little Ice Age (1400–1850 CE), and the Current Warm Period (1850–2000 CE). We then used station-based annual summer precipitation data for the Yangtze River basin (1470 to 2000 CE) to compare precipitation regimes and their intensities between colder (LIA) and warmer (CWP) climates (Fig. 2). Second, we introduced the concept of flood-strong into the flood-generating framework, complementing the widely discussed flood-rich concept in recent studies¹². Flood-rich refers to periods of increased flood frequency, whereas flood-strong denotes episodes of heightened flood intensity. These dimensions represent different aspects of flood regimes and do not necessarily coincide. Accordingly, we depicted both flood-rich (frequency) and flood-strong (intensity) episodes, providing new insights into the structured variability of floods in relation to precipitation regimes and thermodynamic influences. Third, since floods originate from precipitation and vary with underlying landscapes that are subject to human modification, we explicitly considered anthropogenic influences in the analysis of millennium floods in addition to climate change. Given the diversity of landscapes, land use, and land cover changes may yield different impacts, still largely unknown. In combination with compiled demographic data, we isolated and evaluated the anthropogenic influences in terms of basin-wide and downstream effects. The outcomes provide a foundation for building global resilience to alleviate flood risks across the entire basin.

We used unit root tests to distinguish stationarity and non-stationarity in time series data⁵⁴. Specifically, the augmented Dickey–Fuller (ADF) test was applied to examine stationarity (and trends) at a significant level of

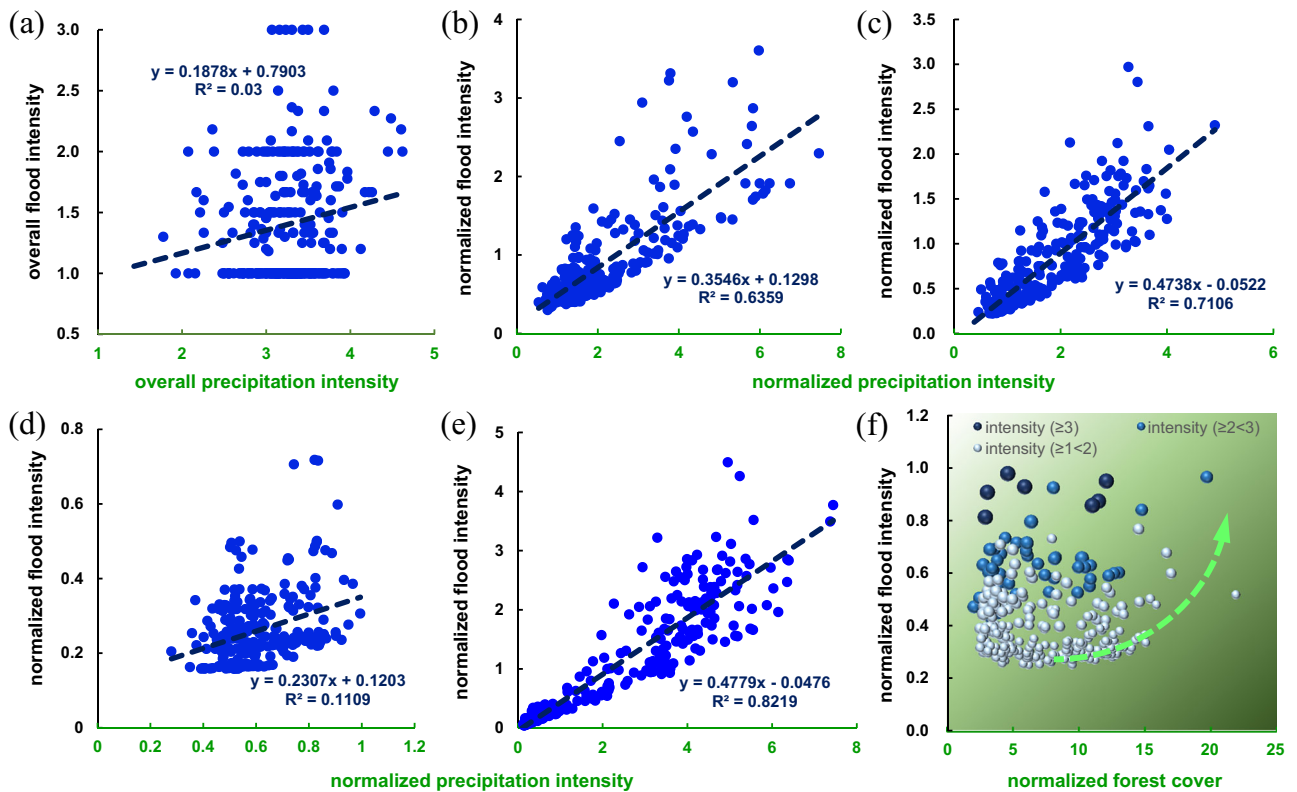


Fig. 5 | Relationships between precipitation and flood intensities in the Yangtze River Basin. a Statistical relationship between overall precipitation and flood intensity. b–e Conditional relationships between precipitation and flood intensity, normalized by population (b), forest cover (c), polder area (d), and their combined effects (e). Normalization accounts for 82.19% of the total impact, with forest cover having the highest influence (71.06%), followed by population (63.59%), and polder

area (11.09%). The regression intercepts suggest that forestation has a positive impact, while population growth and polder construction have negative impacts on flood intensity. f Relationship between flood intensity and forest cover, normalized by precipitation, shows that increased forest cover significantly reduces heavy floods under the same precipitation levels. Bubble sizes represent flood intensity.

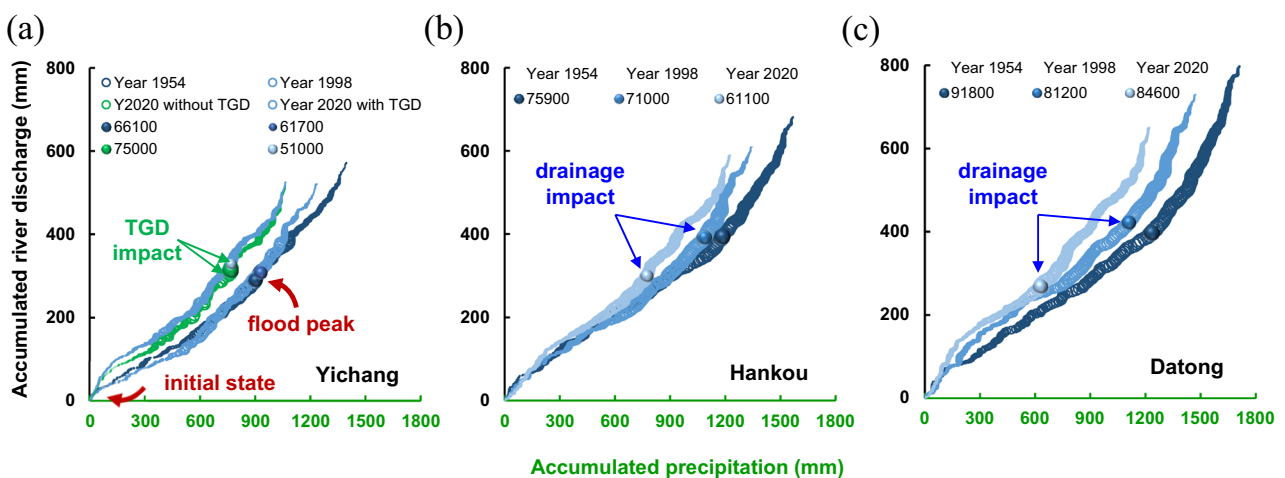


Fig. 6 | Climatic and anthropogenic attribution of three major floods in the Yangtze River Basin. Phase spaces for precipitation and discharge accumulated during the three worst flood events (1954, 1998, 2020) at three representative stations: Yichang (a), Hankou (b), and Datong (c). Accumulation minimizes the variability in flood impact due to antecedent soil moisture conditions. Unlike the 1954 and 1998 events, the 2020 flood occurred with relatively low levels of accumulated precipitation and discharge, underscoring the significant intensification of

downstream flooding due to artificial drainage from 2629 pumping stations in the mid-reaches. Despite the Three Gorges Dam, the world’s largest in terms of power, reducing the flood peak (upstream) from 75,000 m³/s to 51,000 m³/s in 2020 (a), peaks still occurred at Hankou (midstream) and Datong (downstream), with discharges second only to the 1954 event. The size of the bubbles represents the daily river discharge (m³/s), and the solid bubbles indicate the maximum discharge (m³/s) for each flood event.

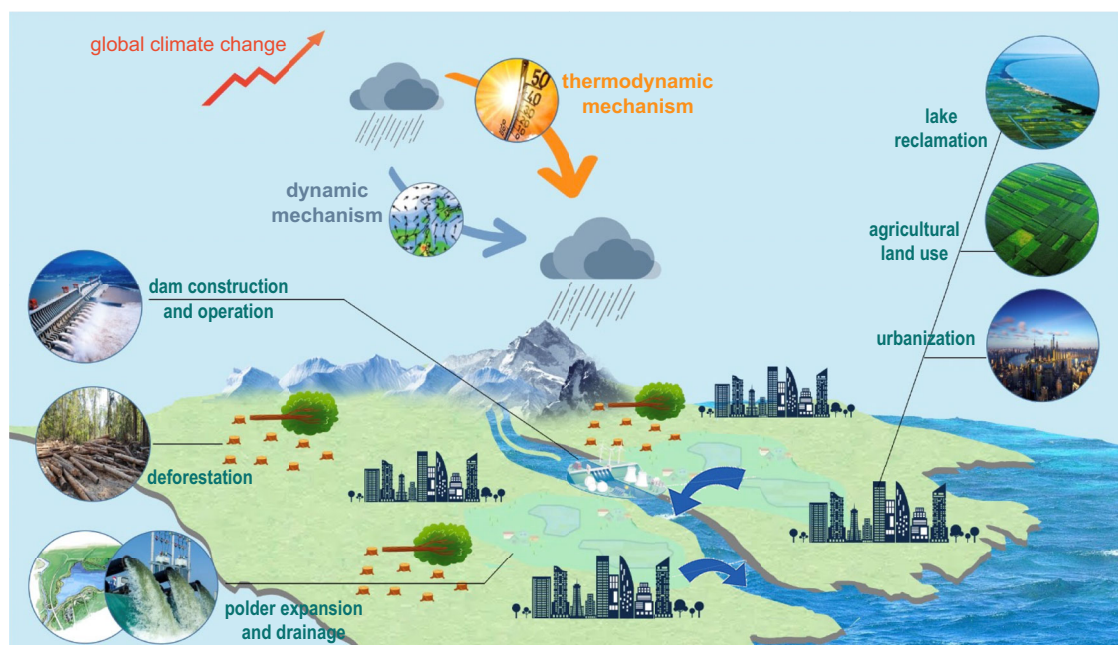


Fig. 7 | Impacts of climate change on regional precipitation patterns and their interactions with human land use in shaping Yangtze River floods. Global climate change influences regional precipitation through dynamic and thermodynamic

mechanisms. Concurrently, human activities, including afforestation/deforestation, agricultural practices, irrigation, polder expansion and drainage, urbanization, and dam construction and operation, alter flood patterns in the basin.

$p = 0.05$ and determine the order of integration for the time series⁵⁵. For non-stationary time series with periodicity, we used the Morlet wavelet approach, which is optimal among many wavelet approaches in determining periodicity⁵⁶. Furthermore, we decomposed the annual flood sum, flooded sub-basin, and overall flood intensity into low- and high-pass filter components—one determined trend and four high-frequency components—for the period 950–2000 CE using the Daubechies-4 algorithms of wavelet analysis⁵⁷ (Fig. S4). The approximate coefficients for the trend were then cointegrated with climate and anthropogenic indicators, including global temperature, precipitation regime, population, forest cover, and polder area. The Johansen test was applied to confirm the multicointegration between the time series⁵⁸. Additionally, we normalized overall precipitation and flood intensities with population, forest cover, polder area, or their combination. The normalization process assigns the precipitation-flood relationship to the same conditions, minimizing differences due to individual or combined influences, thereby allowing for the evaluation of individual influences on the distorted precipitation-flood relationship. Regarding the top three worst flood events (1954, 1998, and 2020), we proposed analyzing the phase space of precipitation and discharge in annual accumulation to minimize the effects of antecedent soil moisture ahead of flood events at three representative stations (Yichang, Hankou, and Datong). Furthermore, the Three Gorges Dam (TGD) outflow was replaced with the TGD inflow to restore the discharge at Yichang for the year 2020, without the TGD.

Data

Hydrological data exists in two forms. First, daily river discharge and water level data are available from the Hydrological Bureau of the Changjiang Water Resources Commission, dating back to 1877 for Yichang, 1865 for Hankou, and 1922 for Datong (with some years missing due to wars). The daily discharge data for the TGD inflow and outflow were obtained from the China Three Gorges Corporation for the period from 1 June 2002 to 31 December 2020. Second, flood events, numerated at three levels (mild, severe, and extreme) for 11 sub-basins, are charted in the Yangtze Chorography for the period from 185 BCE to 1999 CE⁵². To maintain consistency with the precipitation series, we excluded flood events before 950 CE from the analysis.

The precipitation data used for the basin consist of three types: station-based daily, station-based annual summer, and national annual dryness/wetness. First, daily data is available for 179 national meteorological stations from the China Meteorological Data Sharing Service System for the period from 1 January 1951 to 31 December 2020 (Box Fig. 1). Second, station-based annual summer (May–September) precipitation is available from the system for 32 stations within the Yangtze River basin from 1470 to 2000 CE. Precipitation is numerated in five grades from dryness to wetness for each station, according to well-established numeration rules based on extensive compilations of documents routinely recorded in the local chronicles system^{59–61}. Third, the national annual dryness/wetness time series, classified into six modes, was constructed with orthogonal analysis based on 118 stations for the period 1470–1977²⁶ (Fig. S2), extended to the period 950–1991²⁷ and then updated to 2005²⁸.

We extracted global mean surface temperature for the period 950–2000 CE from a 2000-year-long time series of temperature anomalies, using a state-of-the-art dataset reconstructed with a global collection of paleoclimate records⁶². The anomaly is referenced to 13.97°C, the mean for 1961–1990 CE. Annual population data were linearly interpolated from population charts for the basin in each dynasty from 2 CE (Han Dynasty) to 1936 (Republic of China), as documented in historical records⁶³. Annual forest cover was similarly interpolated from forest estimates based on extensive historical documents from the 2nd to the 20th century^{64,65}. Polders, mainly constructed in the mid- and lower reaches of the Yangtze River over the last millennium, were documented, and the annual polder area was linearly interpolated from historical records for the period 950–2000 CE^{66,67}.

Annual reservoir storage and irrigated area data for 1950–2020 CE were collected from published refs. 68–70 and the yearly bulletins for the Yangtze River and the Southwest Rivers⁷¹ (<http://cjw.gov.cn/zwzc/bmgb/szygb/>). Annual population and GDP data for each province are available from the China Statistical Yearbook for the period 1950–2020 CE (<http://www.stats.gov.cn/tjsj/ndsj/>), with the totals for the entire basin calculated subsequently. Electronic drainage power data was estimated based on quantitative descriptions for individual provinces and charts for waterlogging in the basin^{72,73}.

Data availability

The data are available at <https://doi.org/10.57760/sciencedb.12863>.

Received: 29 October 2025; Accepted: 13 January 2026;

Published online: 11 February 2026

References

- Harari Y. N. *Sapiens: A Brief History of Humankind* (HarperCollins Publishers, 2015).
- Schiermeier, Q. Noah's flood. *Nature* **430**, 718–719 (2004).
- Montgomery, D. R. Emperor Yu's great flood. *Science* **353**, 538–539 (2016).
- Mallapaty, S. Pakistan's floods have displaced 32 million people—how researchers are helping. *Nature* **609**, 667 (2022).
- Merz, B. et al. Causes, impacts and patterns of disastrous river floods. *Nat. Rev. Earth Environ.* **2**, 592–609 (2021).
- Teng, J. et al. Flood inundation modelling: a review of methods, recent advances and uncertainty analysis. *Environ. Model. Softw.* **90**, 201–216 (2017).
- Kundzewicz, Z. W. et al. Flood risk and climate change: global and regional perspectives. *Hydrological Sci. J.* **59**, 1–28 (2014).
- Masson-Delmotte, V. et al. *Climate Change 2021: The Physical Science Basis*. (Intergovernmental Panel on Climate Change, 2021).
- Merz, B. et al. Floods and climate: emerging perspectives for flood risk assessment and management. *Nat. Hazards Earth Syst. Sci.* **14**, 1921–1942 (2014).
- Milly, P. C. et al. Stationarity is dead: whither water management?. *Science* **319**, 573–574 (2008).
- Blöschl, G. et al. Changing climate both increases and decreases European river floods. *Nature* **573**, 108–111 (2019).
- Blöschl, G. et al. Current European flood-rich period exceptional compared with past 500 years. *Nature* **583**, 560–566 (2020).
- Knox, J. Large increases in flood magnitude in response to modest changes in climate. *Nature* **361**, 430–432 (1993).
- Lombardi, R., Davis, L. & Therrell, M. D. Flood variability in the common era: a synthesis of sedimentary records from Europe and North America. *Phys. Geogr.* **42**, 1890894 (2021).
- Wilhelm, B. et al. Impact of warmer climate periods on flood hazard in the European Alps. *Nat. Geosci.* **15**, 118–123 (2022).
- Zhou, L. et al. Extreme floods of the Changjiang River over the past two millennia: contributions of climate change and human activity. *Mar. Geol.* **433**, 106418 (2021).
- Munoz, S. E. et al. Climatic control of Mississippi River flood hazard amplified by river engineering. *Nature* **556**, 95–98 (2018).
- Calder, I., Smyle, J. & Aylward, B. Debate over flood-proofing effects of planting forests. *Nature* **450**, 945 (2007).
- FAO, CIFOR. *Forests and floods: drowning in fiction or thriving on facts?* (RAP Publication, 2005).
- Blöschl, G. et al. Increasing river floods: fiction or reality?. *WIREs Water* **2**, 329–344 (2015).
- Bathurst, J. C., Fahey, B., Iroumé, A. & Jones, J. Forests and floods: using field evidence to reconcile analysis methods. *Hydrological Process.* **34**, 3295–3310 (2020).
- Harden, T. M. et al. *Historical and paleoflood analyses for probabilistic flood-hazard assessments*. (U.S. Geological Survey, 2021).
- Winsemius, H. C. et al. Global drivers of future river flood risk. *Nat. Clim. Change* **6**, 381–385 (2016).
- Hu, F., Tan, D. & Xu, Y. *Yangtze Water Risks, Hotspots and Growth*. (China Water Risk, 2019).
- Zhou, X., Zhao, P., Liu, G. & Zhou, T. Characteristics of decadal-centennial-scale changes in East Asian summer monsoon circulation and precipitation during the Medieval Warm Period and Little Ice Age and in the present day. *Chin. Sci. Bull.* **56**, 3003–3011 (2011).
- Wang, S. & Zhao, Z. An analyses of historical data of droughts and floods in last 500 years in China. *Acta Geogr. Sin.* **34**, 329–341 (1979).
- Wang, S., Zhao, Z. & Chen, Z. *Flood and Drought Disasters and Its Diagnosis in the Yangtze and the Yellow Rivers*. (China Meteorological Press, 1993).
- Wang, S. & Huang, J. The variations of geographical latitude of rain belts in summer over Eastern China during the last millennium. *Adv. Clim. Change Res.* **2**, 117–121 (2006).
- Emori, S. & Brown, S. Dynamic and thermodynamic changes in mean and extreme precipitation under changed climate. *Geophys. Res. Lett.* **32**, L17706 (2005).
- Marvel, K. D. & Bonfils, C. J. Identifying external influences on global precipitation. *Proc. Natl. Acad. Sci.* **110**, 19301–19306 (2013).
- Chen, G. et al. Thermodynamic and dynamic mechanisms for hydrological cycle intensification over the full probability distribution of precipitation events. *J. Atmos. Sci.* **76**, 497–516 (2019).
- Yang, J. et al. Asynchronous variation in the holocene asian monsoon recorded by marine sediments and its implication. *Front. Earth Sci.* **12**, 1493790 (2025).
- Du, Y., Xie, Z., Wang, N., Miao, Q. & Zhang, L. Influence of zonal variation of the subtropical westerly jet on rainfall patterns and frequency of heavy precipitation events over East Asia. *J. Clim.* **35**, 6611–6626 (2022).
- Cherchi, A. et al. The response of subtropical highs to climate change. *Curr. Clim. Change Rep.* **4**, 371–382 (2018).
- Carleton, A. M., Birkel, S. D. & Saros, J. E. 2000 years of North Atlantic-Arctic climate. *Quat. Sci. Rev.* **216**, 1–17 (2019).
- Geng, T., Yang, Y. & Wu, L. On the mechanisms of Pacific decadal oscillation modulation in a warming climate. *J. Clim.* **32**, 1443–1459 (2019).
- Ford, H. L., Ravelo, A. C. & Polissar, P. J. Reduced El Niño-Southern oscillation during the last glacial maximum. *Science* **347**, 255–258 (2015).
- Pontes, G. et al. Mid-Pliocene El Niño/Southern oscillation suppressed by Pacific intertropical convergence zone shift. *Nat. Geosci.* **15**, 726–734 (2022).
- Pall, P., Allen, M. R. & Stone, D. A. Testing the Clausius-Clapeyron constraint on changes in extreme precipitation under CO₂ warming. *Clim. Dyn.* **28**, 351–363 (2007).
- Liu, J., Wang, B., Cane, M., Yim, S. Y. & Lee, J. Y. Divergent global precipitation changes induced by natural versus anthropogenic forcing. *Nature* **493**, 656–659 (2013).
- Visser, J. B., Wasko, C., Sharma, A. & Nathan, R. Eliminating the “Hook” in precipitation-temperature scaling. *J. Clim.* **34**, 9535–9549 (2021).
- Yin, H. & Li, C. Human impact on floods and flood disasters on the Yangtze River. *Geomorphology* **41**, 105–109 (2001).
- Linsley, R. K. The relation between rainfall and runoff: review paper. *J. Hydrol.* **5**, 297–311 (1967).
- Berghuijs, W. R., Woods, R. A., Hutton, C. J. & Sivapalan, M. Dominant flood generating mechanisms across the United States. *Geophys. Res. Lett.* **43**, 4382–4390 (2016).
- McClymont, K., Morrison, D., Beevers, L. & Carmen, E. Flood resilience: a systematic review. *J. Environ. Plan. Manag.* **63**, 1151–1176 (2020).
- Zhang, J. M. & Lu, X. Q. *Historic Human Activity and Environmental Change in the Middle Reaches of the Yangtze River*. (Wuhan University Press, 2011).
- Xu, Z. F. & Xu, G. J. *Flood Prevention, Yangtze Chorography*. (Encyclopedia of China Publishing House, 2003).
- Mao, Z. P. *History of Water Conservancy in the Yangtze River*. (Changjiang Press, 2019).
- Hu, X., Liu, J., Wu, J. & Ma, Q. Influence of drainage of pumping stations along middle and lower reaches of Yangtze River on flood control of main stream. *Yangtze River* **51**, 172–178 (2020).
- Sornette, D. & Ouillon, G. Dragon-kings: mechanisms, statistical methods and empirical evidence. *Eur. Phys. J. Spec. Top.* **205**, 1–26 (2012).

51. IPCC Working Group I. *IPCC WGI Interactive Atlas*. <https://interactive-atlas.ipcc.ch/> (2022).
52. CWRC-MWR. *Yangtze Chorography*. (Encyclopedia of China Publishing House, 2005).
53. Maddison, A. *Chinese Economic Performance in the Long Run: 960–2030 AD*. (OECD, 2007).
54. Kirchgässner, G., Wolters, J. & Hassler, U. *Introduction to Modern Time Series Analysis*. (Springer-Verlag, 2013).
55. Ogaki, M. Unit roots in macroeconometrics: a survey. *BOJ Monetary Econ. Stud.* **11**, 131–154 (1993).
56. Khaliq, M. N., Ouarda, T. B. M. J., Ondo, J.-C., Gachon, P. & Bobée, B. Frequency analysis of a sequence of dependent and/or non-stationary hydro-meteorological observations: a review. *J. Hydrol.* **329**, 534–552 (2006).
57. Addison, P. S. *The Illustrated Wavelet Transform Handbook*. (CRC Press, 2017).
58. Martinez, W. L. & Martinez, A. R. *Computational Statistics Handbook with MATLAB*. (CRC Press, 2016).
59. CAMS. *Yearly Charts of Dryness/Wetness in China for the Last 500-Year Period*. (SinoMaps Press, 1981).
60. Zhang, D. E. & Liu, C. Z. A supplement to yearly charts of dryness/wetness in China for the last 500-Year Period (1980–1992). *Meteorol. Mon.* **19**, 41–45 (1993).
61. Zhang, D. E., Li, X. Q. & Liang, Y. Y. A further supplement to yearly charts of dryness/wetness in China (1993–2000). *J. Appl. Meteorol. Sci.* **14**, 379–384 (2003).
62. PAGES 2k Consortium Consistent multidecadal variability in global temperature reconstructions and simulations over the Common Era. *Nat. Geosci.* **12**, 643–649 (2019).
63. Zhang, G. X. *History of Population Development in the Yangtze River Basin*. (Hubei Education Press, 2006).
64. Zhou, H. W. *Forest Change and Soil Erosion in the Yangtze River Basin*. (Hunan Education Publishing House, 2006).
65. Miller Ian, M. *Fir and Empire: The Transformation of Forest in Early Modern China*. (University of Washington Press, 2020).
66. Mei, L., Zhang, G. X. & Yan, C. G. *Investigation on Development of the Two-Lake Plain*. (Jiangxi Education Publishing House, 1995).
67. Huang, J. W. *Coevolution of the Human-water Relationships in the Mid-Yangtze Reaches*. (Hubei People's Publishing House, 2010).
68. Deng, J. Change of effective irrigation areas in the Yangtze River Basin. *Express Water Resour. Hydropower Inf.* **19**, 26–28 (1998).
69. Chen, J. et al. Changes in monthly flows in the Yangtze River, China – with special reference to the Three Gorges Dam. *J. Hydrol.* **536**, 293–301 (2016).
70. Zhang, X. & Yao, F. Effective water saving irrigation in the Yangtze River basin. *Water Sav. Irrig.* **2**, 101–104 (2016).
71. CWRC-MWR. *Changjiang and Southwest Rivers: Water Resources Bulletin*. (2006–2020).
72. DRWCSC-MWR. *Pumping Station in China*. (China Water & Power Press, 1993).
73. Liu, Q. Q. & Yang, Z. J. Review on planning of water logging control in Yangtze River Basin. *Yangtze River* **44**, 59–62 (2013).

Acknowledgements

We thank Prof. Hesheng Chen for his long-term support in studying the Yangtze River floods and Prof. Jian Liu for her comments on an earlier version of the manuscript. This work was supported by the National Natural Science Foundation of China (Grant nos. 42230112, 41430855).

Author contributions

Y.B.L. conceived of the work, led the study, completed the analysis, and wrote the manuscript with inputs from all co-authors. J.W. supported the manuscript writing process and highlighted the key outcomes of the study. G.S. and S.G.M. provided feedback, edits and revisions. Y.W.L. and H.Z. compiled and quality checked the data. C.L. made illustrations.

Competing interests

The authors declare no competing interests.

Additional information

Supplementary information The online version contains supplementary material available at <https://doi.org/10.1038/s44304-026-00169-9>.

Correspondence and requests for materials should be addressed to Yuanbo Liu or Jianguo Wu.

Reprints and permissions information is available at <http://www.nature.com/reprints>

Publisher's note Springer Nature remains neutral with regard to jurisdictional claims in published maps and institutional affiliations.

Open Access This article is licensed under a Creative Commons Attribution-NonCommercial-NoDerivatives 4.0 International License, which permits any non-commercial use, sharing, distribution and reproduction in any medium or format, as long as you give appropriate credit to the original author(s) and the source, provide a link to the Creative Commons licence, and indicate if you modified the licensed material. You do not have permission under this licence to share adapted material derived from this article or parts of it. The images or other third party material in this article are included in the article's Creative Commons licence, unless indicated otherwise in a credit line to the material. If material is not included in the article's Creative Commons licence and your intended use is not permitted by statutory regulation or exceeds the permitted use, you will need to obtain permission directly from the copyright holder. To view a copy of this licence, visit <http://creativecommons.org/licenses/by-nc-nd/4.0/>.

© The Author(s) 2026